RECENT PROGRESS IN THE ASSESSMENT OF IRRADIATION EFFECTS FOR IN-VESSEL FUSION MATERIALS: TUNGSTEN AND COPPER ALLOYS

D. Terentyev[1], M. Rieth[2], G. Pintsuk[3], J. Riesch[5], A. Von Muller[4], S. Antusch[2], K. Mergia[5], E. Gaganidze[2], H.-C. Schneider[2], M. Wirtz[3], S. Nogami[6], J. Coenen[3], J.H. You[4], A. Zinovev[1], W. Van Renterghem[1]

[1]Belgian Nuclear Research Centre, SCK•CEN, Mol, 2400, Belgium
[2]Karlsruhe Institut für Technologie, Hermann-von-Helmholtz-Platz 1, 76344 Eggenstein-Leopoldshafen, Germany
[3]Forschungszentrum Jülich GmbH, Institut für Energie- und Klimaforschung – Plasmaphysik, 52425 Jülich, Germany
[4]Max-Planck-Institut für Plasmaphysik, 85748 Garching, Germany
[5]NCSR Demokritos, Institute of Nuclear and Radiological Science and Techology, Energy and Safety, 15310 Agia Paraskevi, Greece
[6]Tohoku University, 6-6-01-2, Aramaki-aza-Aoba, Aoba-ku, Sendai, 980-8579, Japan

Abstract

The present contribution highlights results of the recent irradiation campaigns applied to screen mechanical properties of advanced tungsten and copper-based materials – main candidates for the application in the plasma-facing components (PFC) in the European DEMO. The main challenges in the formulated irradiation programme were linked to: (I) assessment of the ductile-to-brittle transition temperature (DBTT) of newly developed tungsten-based materials; (ii) investigation of an industrial pure tungsten grade under high temperature irradiation, reflecting operational conditions in the high flux divertor region; (iii) assessment of the high temperature strength of CuCrZr-based alloys and composites developed to enable the extension of the operational window for the heat sink materials. The development and choice of the advanced materials is driven naturally by the need to extend the operation temperature/fluence window thereby enlarging the design space for PFCs. The obtained results helped identifying the prospective tungsten and copper-based material grades as well as yielded a number of unexpected results pointing at severe degradation of the mechanical properties due to the irradiation. The results are discussed along with the highlights of the microstructural examination. An outlook for near future investigations involving in-depth post-irradiation examination and further irradiation campaigns is provided.

1. INTRODUCTION

DEMO and fusion power plants beyond it require robust materials to ensure durable and safe operation as well as commercially competitive construction and dismantling design. One of the main challenges in the development of those materials is the assessment of irradiation effects, originating from the nuclear fusion reaction, which generates 14 MeV neutrons damaging the materials atomic lattice. So called in-vessel materials will experience the most severe neutron exposure being far beyond the damage limits acquired by currently operating nuclear power plants. The task of development and qualification of the in-vessel materials thus boils down to securing that the degradation of mechanical, thermal and physical properties will remain within acceptable limits, which are in turn driven by the design of components and operational scenario. Overall, three main functions of the in-vessel materials can be singled out, such as: structural (steel), armour (tungsten) and heat sink (copper). For some materials the function can be mixed, i.e. heat sink and structural for the copper pipe.

The assessment of the irradiation effects in candidate DEMO in-vessel materials is one of the priorities within European materials programme [1]. This contribution highlights the recent efforts done for the armour and heat sink materials, in particular for the application in the high flux divertor region. Based on the already available knowledge (see e.g. [2-5] and references cited therein), the operational conditions for the baseline tungsten and copper materials are tentatively determined as illustrated on Fig. 1. For each of the baseline materials, the lower temperature bound is defined by the embrittlement (fracture without plastic deformation), while the upper temperature bound is determined by softening of the material (reduction of the yield point). Accordingly, the main challenges in the formulated irradiation programmes were linked to: (I) assessment of the ductile-to-brittle transition temperature (DBTT) of baseline tungsten and advanced tungsten composites; (ii) investigation of baseline tungsten under irradiation at very high temperature, reflecting operational conditions in the high flux divertor region; (iii) assessment of the mechanical properties of CuCrZr-based alloys and composites. The choice of the advanced materials is driven naturally by the need to extend the operation temperature/fluence window to extend the design space. Here, we present the most recent results obtained for a number of tungsten and copper-

based alloys identified thanks to down-selection on the basis of preliminary tests so fat not involving neutron irradiation.

The neutron exposure was realized in the Belgian Material Test Reactor (BR2), and the irradiation capsules were placed directly inside the fuel elements to minimize the generation rate of Re/Os transmutation due to thermal neutrons coming closer to fusion relevant conditions with a high energy neutron spectrum. The target irradiation fluence was defined as 1 dpa (in W) corresponding to the expected damage at end-of-operation of ITER. Extraction of the properties of the neutron exposed materials involved extensive post irradiation examination (PIE) campaigns in Germany, Belgium, and Greece.

2. INVESTIGATED MATERIALS AND METHODOLOGY

The basic information about the materials investigated here is summarized in Table 1. More information about the fabrication route, microstructure and mechanical properties in the non-irradiated state can be found in the references provided in the table. The samples were manufactured to their final shape by the material suppliers, as specified in the table, except the reference tungsten, for which the samples were fabricated using the electric discharge machine at SCK•CEN.

Neutron irradiation on the various materials and specimen shapes was performed in BR2 inside the fuel element in the position close to the center of the reactor and in the mid-plane with the average fast neutron (E > 1 MeV) flux of 1×10^{14}n/cm^2/s at a power of 60 MW. The samples were encapsulated in a steel tube with 1.5 mm wall thickness filled with He. The gap between the samples and the pressure tube was adjusted to achieve a target temperature during the irradiation following thermal and neutronic calculations. According to a finite element analysis of thermal flow, variation of 25-50°C occurred during the irradiation cycle (the lower the absolute irradiation temperature, the lower its in-cycle variation) due to the burnup of the fuel element. The irradiation dose was calculated by MCNPX 2.7.0 [6]. The dpa cross sections for W have been prepared from the JENDL4 file (MT444) for the threshold displacement energy of 55 eV, following the recommendation of IAEA [7]. The transmutation of Re and Os was calculated based on the ALEPH code developed by SCK•CEN and available nuclear databases [8-12]. The typical transmutation rate from W to Re was about 1.8-2 at.% per dpa. The irradiation duration was between 143 and201 reactor operational days depending on the position of the capsule in the reactor channel. The irradiation dose on tungsten samples was 1.04-1.25 dpa (in W), and on copper-based materials 1.02- 1.25 dpa (in W).

Pre- and post-irradiation examination via mechanical tests was conducted using certified equipment in hot cells in the premises of the research centers KIT and SCK•CEN in Germany and Belgium, respectively. The mechanical characterization comprised fracture toughness, tensile and three-point bending tests. Detailed information on the test conditions, sample geometries, and procedures can be found in [13-15]. Most essential information on the test procedures is summarized below.

Uniaxial tensile tests were performed on mini flat dog-bone shaped specimens with the length of 16 mm, a gauge length of 5.2 mm and an effective cross section of 2.4 mm^2. The strain was calculated based on the measurements of the pull rod displacement using linear variable differential transformer (LVDT). The LVDT and the load cell were calibrated according to the required standards on the equipment applied to test both irradiated and reference samples. Tests were performed according to the ASTM E8 guidelines.

Miniaturized three-point bending (3PB) specimens were tested using the configuration according to the ASTM standard E290 [16]. The span between the lower supporting pins was 8.5 mm and their diameter was 2.5 mm. The samples had dimensions 1×1×12 mm^3 with a polished surface. L-T orientation was applied for the textured materials (i.e. tungsten plates and tungsten rod). Tensile and bending tests were performed at SCK CEN in air.

Fracture toughness measurements were performed using 3PB and disk-shaped compact tension (DCT) specimens with a narrow notch with a root radius around 50 µm cut by EDM. Fracture toughness samples were machined in the T-L orientation. The T-L orientation for the fracture toughness assessment has been selected in accordance with the texture of PFC ITER components (i.e. thermal stresses act normal to the rolling direction). The test temperature for irradiated specimens ranged from RT up to 1100°C at KIT using a vacuum furnace, and up to 580°C in air at SCK CEN. K_Q values (linear elastic stress intensity factor) were calculated according to the requirements of ASTM E399 [17]. Eq. (1) is used for the determination of the fracture toughness K_Q for mode I fracture:

$$K_Q = \frac{P_Q}{B\sqrt{W}} \cdot f\left(\frac{a}{W}\right), \quad (1)$$

where P_Q is defined either as the load at fracture in case of the absence of plastic deformation or as the load at the intersection of the loading curve with the straight line exhibiting a slope that is 95% of the elastic slope in case plastic deformation occurs; $f\left(\frac{a}{W}\right)$ is a geometry dependent function related to the ratio between the crack size a and the width W, which can be found in the standard; B is the specimen thickness.

Table 1. Summary of information on the advanced materials. Coloumn "Reference" points to earlier works where the microstructure and mechanical properties of a corresponding material were investigated.

Material **Form of product** **Supplier.**	**Reference, ID used in paper**	**Advantages / selection criteria**
Pure W (IGP) Forged bar, 36×36 mm cross-section Plansee AG (Austria)	[15, 18] IGP	Industrial material grade, well-established fabrication methodology, numerous experimental data available.
K-doped W and K-doped W/Re (3%Re) Hot-rolled plates, d = 7 mm Tohoku Univ (Japan).	[19, 20] W-K (Tohoku) W-Re-K (Tohohku)	Industrial material, established fabrication methodology, engineering-relevant plate thickness is available, low DBTT. Potential tolerance to the irradiation damage thanks to fine-grain structure. Improved resistance against recrystallization.
Powder injection molded W with TiC and Y_2O_3 particle reinforcement Disks/plates, d = 4 mm KIT (Germany)	[21] PIM W-TiC PIM W-Y2O3	Net-shape component production, flexibility on the micro-alloying, up-scalable fabrication methodology. Improved resistance against recrystallization.
K-doped cold-rolled W Plate, d = 1 mm KIT (Germany).	[22] W-K (KIT)	Unique combination of ductility, strength and low DBTT. Potential tolerance to the irradiation damage thanks to fine-grain structure. Improved resistance against recrystallization.
CuCrZr-W laminates (W-27wt.%CuCrZr) Plate, d = 1 mm KIT (Germany).	[23, 24] CuCrZr-W_L	Unique combination of ductility, strength and low DBTT. High potential for large scale production.
W fiber reinforced CuCrZr (46 wt.%) Discs, Wf ∅ = 145 µm, d = 1 mm IPP Garching & FZJ (Germany).	[25-27] CuCrZr-W_f	Pseudo-ductility and toughness due to the crack-deflection mechanism. Potential tolerance to the irradiation damage due to highly ductile and fine-grain structured W fibers.
W particle-reinforced CuCrZr (30 wt.%) Plate. IPP Garching (Germany).	[28] CuCrZr-W_P	High-temperature strength thanks to tough tungsten particles. Low temperature ductility thanks to the ductile CuCrZr matrix.

Copper strengthened by Y_2O_3 ODS particles and V-added precipitates (Cu-0.922%Cr-0.041%Zr-0.221%V, wt.%). supplied by KIT (Germany).	Cu-ODS CuCrZr-V	High temperature strength thanks to the precipitation strengthening.

3. RESULTS AND DISCUSSION

3.1. Tungsten-based materials

3.1.1. Baseline commercial pure tungsten

Assessment of the fracture toughness and associated irradiation embrittlement of tungsten is one critical gap in the tungsten material database and the related DEMO material property handbook under development [1]. Fig. 2 summarizes the currently obtained results for pure tungsten irradiated at 600, 800, 900 and 1200°C. The fracture toughness samples had T-L orientation with grains elongated perpendicular to the crack propagation direction. The DBTT of the non-irradiated tungsten with this grain orientation is about 400°C. Fig. 2(a) shows the evolution of the fracture toughness K_Q, which exhibits a steep rise near 400°C as the load-displacement response reveals transition from pure elastic to elasto-plastic deformation, see the inset figure. The lower shelf fracture toughness is ~7-10 MPa·$m^{0.5}$, i.e. in the range of the values obtained for other tungsten products tested in the brittle state [29-31]. After irradiation at 800°C, the onset of the plastic deformation shifts to 1025°C (see invalid value of K_Q at 1025°C, and load-displacement curves as well as in-depth discussion in Ref. [13]). K_Q measured at 800°C is just slightly above 10 MPa·$m^{0.5}$ implying that the material's fracture toughness is as low as the one of non-irradiated material in the lower shelf, i.e. the material is practically brittle. A set of tests performed at 500-580°C for the same material irradiated at 900 and 1200°C has also revealed fully brittle fracture, confirming that the irradiation at high temperature still provokes non-negligible embrittlement, see Fig. 2(b). The samples irradiated to a lower dose (i.e. 0.2 dpa) were tested at 600°C and some limited plastic deformation was seen. Hence, it could be concluded that the DBTT shift for 0.2dpa_600°C is about 200°C, while for 1.25dpa_800°C it increases to 625°C. The high temperature (> 600°C) test programmes are ongoing to deduce the transition temperature at the other investigated irradiation temperatures.

SEM images of the fracture surface are provided in Fig. 3 for the samples tested at 500 and 580°C. In the non-irradiated state [14], the fracture surface of this material above 500°C is characterized by the presence of intergranular ductile fracture and dimples. The signature of brittle intergranular fracture is seen already at 0.2dpa_600°C, as shown in Fig. 3(a) and (b), although intergranular dimples are also seen. At 1.16-1.18 dpa, the fracture surface often encounters regions featuring transgranular fracture showing the suppression of the intra-granular ductile deformation by the irradiation defects. To shed a light on the type of the microstructural damage, we provide a series of TEM micrographs (see Fig. 4) taken from the lamellas directly extracted from the fracture toughness samples (see schematics on Fig. 3). The microstructure of 0.2dpa_600°C irradiated sample is presented on the upper pane of Fig. 4. The irradiation did not have any remarkable impact on the sub-grain structure and dislocation line density. The newly formed defects were thus dislocation loops and voids. The majority of the loops are of a/2<111> type (fraction of a<100> loops is less than 5%). Loop density is $(1.2\pm0.3)\times10^{23}/m^2$ and average size is 3.9±1.1 nm, see example of the loop pattern on Fig. 4(a). Some dislocations lines appear to be strongly decorated by the loops as shown in Fig. 4(b). The voids are small (mean size is 0.79±0.11 nm) and numerous (density is $6.5\times10^{23}/m^3$), the corresponding TEM image is given in Fig. 4(c). Given the limited Re/Os transmutation at 0.2 dpa (0.4at.%Re, 0.02at.%Os), the presence of precipitates is not expected and was not identified by the applied TEM analysis. Also, the observed microstructure is in good agreement with the one found by Hasegawa et al. under similar irradiation conditions (0.15-0.17 dpa, 600-800°C) [32, 33]. At high dpa/high irradiation temperature, the voids are much more pronounced, such that at 1.18_900°C the void size ranges from few up to 15 nm with a mean value of 6 nm, Fig. 4(d). At 1200°C, the mean size of voids is about 4 nm and upper size reaches ~10 nm. Important to mention that dislocation loops are also present in the samples irradiated at 900 and 1200 °C (see Fig. 4(e)), however, their density is considerably lower than what is observed at 0.2dpa_600°C. The reduction of the loop density with the increase of the irradiation temperature above 800°C is also fully consistent with the recent TEM studies applied to various neutron irradiated tungsten grades [34, 35]. Finally, one should also expect the presence of non-coherent phases at the high irradiation temperature and ~1 dpa damage level (e.g. see review of Rieth [2] and references cited therein). Revealing and characterizing these precipitates as

well as possible segregation zones implies an advanced microstructural analysis using multiple TEM-EDX detectors and atom probe techniques, which is the next planned investigation step.

3.1.2. Advanced tungsten materials

The screening assessment of the irradiation effects in the advanced tungsten materials was performed using mini-bend samples. The primary objective was to clarify, which materials would remain ductile within the 600°C threshold after the irradiation exposure up to ~1 dpa at 600 and 1100°C. The flexural stress-strain diagram for the non-irradiated materials is presented in Fig. 5(a), showing an example of the performance at 600°C. The change of the response after the irradiation at 600 and 1100°C is shown, respectively, in Fig. 5(b) and (c). The curves clearly show a significant irradiation hardening (i.e. increase of the stress level corresponding to the transition from elastic to plastic deformation) with still remaining ductility in all materials except the two PIM grades. Fracture of the PIM materials turned out to be fully brittle, also confirmed by SEM investigation, though not provided here. The amplitude of the irradiation hardening depends on the irradiation temperature and it is evidently lower for 1100°C, for instance the apparent yield point (inflection form linear to plastic deformation) increases by a factor of two. The latter is correct for most of the tested materials, but not for K-doped(KIT) which might be linked with fine-grain microstructure that renders low work-hardening capacity. It is clear that the plate products (i.e. W-K and W-Re-K) as well as reference W bar (IGP) exhibit ductility at 580°C after the irradiation in both conditions. To determine the DBTT, bending tests were conducted at lower temperature.

The DBTT criterion is adopted from [14]. T_{DBTT} is obtained by fitting the flexural strain at fracture (*FS*) vs. test temperature through setting upper threshold strain (FS_{top}) as 10% and the lower strain (FS_{base}) as 0%, with the equation:

$$FS(T) = \frac{10\%}{1+exp\left(C(T_{DBTT}-T)\right)} \quad (2)$$

where *C* is the slope of the transition curve; T is the test temperature. In this case, T_{DBTT} corresponds to the mean strain at fracture being 5%, which is also the criterion proposed in [36]. Note that *FS(T)* is the plastic flexural strain defined by subtracting the elastic strain from the load-displacement curve. *FS* vs. temperature is displayed in Fig. 6 for the cold-rolled 1 mm W plate (KIT), the reference W bar (IGP) and both 7 mm K-doped W and W/Re plate products. Given the upper test temperature of 580°C, T_{DBTT} could not be determined for the PIM W grades (not shown on Fig. 6) the W-Re-K plate as well as IGP W irradiated at 600°C, as in all those cases it apparently lies above 600°C.

Table 2 and Fig. 7 summarize the DBTT values and related error, which is defined as temperature range where the plastic flexural strain at fracture exceeds 5% (hence, it depends on the density of points near the DBTT). Note that the bend samples were tested in L-T orientation, which is why T_{DBTT} (IGP) is much lower than the one determined for the T-L orientation in Fig. 2(a). Fig.7 reveals that ΔDBTT has a strong dependence on the irradiation temperature. The K-doped 7 mm plate exhibits the smallest DBTT shift of ~250°C at both irradiation temperatures. The addition of 3 at.%Re yields to a considerable increase of the DBTT at T_{irr}=600°C, which demonstrates that there is a measureable effect of Re (and its transmutation to Os) causing irradiation induced material modifications and related material degradation.

The DBTT shift in the cold-rolled K-doped 1 mm plate is 375°C, and it is 400°C for the reference W bar at T_{irr}=1100°C, while at T_{irr}=600°C both materials exhibit DBTT at or exceeding 600°C, which needs in both cases further experimental clarification. Combining the results of the bending tests with the data presented in Fig. 2 for the reference W bar (IGP), one can assign a temperature range of 900-1100°C as the temperature range in which under irradiation conditions of 1 dpa and a Re generation rate of 2 at.%/dpa the DBTT of this material would still stay below this temperature . With this respect, the DBTT of K-doped 7 mm plate (Tohoku), irradiated at the same conditions as IGP, is only 325 ± 50 °C, which indicates a reduction of the lower bound for the acceptable operational temperature range under the given conditions to at least 600°C.

Table 2. DBBT (corresponding to 5% mean fracture strain) values obtained using Eq.2 and *FS* data presented in Fig.6.

Material	T_{DBTT} in non-irradiated state	T_{DBTT} at T_{irr}=600°C	T_{DBTT} at T_{irr}=1100°C
K-doped cold-rolled plate 1mm (KIT), L-S orientation, Fig.6(a)	150 ± 50 °C	~ 600 °C, to be confirmed by high T tests	525 ± 75 °C

W bar (IGP) L-T orientation, Fig.6(b)	150 ± 25 °C	> 600 °C	550 ± 50 °C
K-doped rolled plate 7mm (Tohoku), L-S orientation,Fig.6(c)	75 ± 25 °C	325 ± 50 °C	325 ± 25 °C
K-doped 3at.%Re-alloyed rolled plate 7mm (Tohoku), L-S orientation, Fig.6(d)	0 ± 25 °C	> 600 °C	350 ± 100 °C

3.2. Advanced copper-based materials

Presentation of the results obtained for the Cu-based materials will comprise the data obtained at the upper and lower boundary of the irradiation and test temperatures i.e. 150 and 450°C, as this will allow assessing the extension of the low-temperature embrittlement and high temperature softening. Fig. 8(a) shows the engineering stress-strain curves for the non-irradiated materials, Fig. 8(b) and (c) shows these curves, at $T_{irr}=T_{test}=150°C$ and $T_{irr}=T_{test}=450°C$, respectively. The main observed irradiation induced effects are a reduction of total elongation seen for all tested materials at 150°C, embrittlement observed for the Cu-W laminates, and strength reduction for the CuCrZr-V at 450°C.

The stress-strain response at test temperature of 150°C is compared for CuCrZr-Wf, CuCrZr-W_l and Cu-ODS materials in Fig. 9(a,b,c) for all three investigated irradiation temperatures. For the Cu-Wf, Fig. 9(a), the main effect of the irradiation is expressed in considerable irradiation hardening i.e. the rise of UTS by a factor of two and only moderate reduction of the elongation. By increasing the irradiation temperature from 150°C up to 450°C, the elongation partially recovers without any significant change in the UTS. Fig. 10 provides SEM micrographs of the fracture surface of reference and 150°C-irradiated samples, both tested at 150°C. The specimens are characterized by less necking and a related lower reduction of area in the irradiated sample, i.e. compare Fig. 10(a) and (b). Close inspection of the tungsten fibers surface reveals that after the irradiation several fibers fractured in a brittle manner such as one shown in Fig. 10(c). Other fibers exhibit typical fracture pattern registered in the non-irradiated fibers tested individually at RT and elevated temperatures [37]. The surrounding copper matrix is deformed in a ductile mode by dimple rupture.

CuCrZr-W_L samples (see Fig.9b) exhibit no ductile deformation when tested at 150°C after the irradiation at 150, 350 or 450°C. In fact, very similar results were found at other test temperature. The fracture surface of reference and 150°C-irradiated samples tested at 150°C are shown in Fig. 11. The fracture of the reference sample occurs by the delamination and necking of individual tungsten grains (fully in line with ref.[23]), see Fig. 11(a),while the copper interlayers exhibit fracture by dimple rupture. After the irradiation, Cu-interlayers still show ductile deformation with well-resolved dimples, while W foils exhibit brittle intergranular fracture with large lateral cracks emerging near the W-Cu interfaces. Examples of such cracks are shown for two different fracture areas on Fig. 11(c) and (d). The irradiation embrittlement of Cu-W laminates has been already reported by Garrison et al. [38], however, the irradiation was performed under conditions (HFIR, Rabbit) causing a higher Re/Os generation rate in tungsten, and higher irradiation temperature (400-800°C) was explored. The present results confirm the irradiation embrittlement.

The Cu-ODS material (see Fig.9c) exhibits at T_{irr} = 150°C considerable hardening (UTS increase by 80%) and zero uniform elongation, although the post-necking elongation yields to 8%. Increasing the test temperature up to 450°C leads to the progressive reduction of the UTS and recovery of the total and uniform elongation.

The tensile data for the V-CuCrZr are presented in Fig. 9(d), and there we focus on the response after the irradiation at 450°C due to the apparent loss of strength and ductility. For reference, the response of the material in its non-irradiated state is also presented. After irradiation, the UTS drops from 350 MPa down to 130 MPa. The reduction of the test temperature to 150°C leads to the UTS value of 220-230 MPa – being still much lower than the UTS in the non-irradiated state. Apparently, the 450°C irradiation has modified the structure and/or size/density distribution of strengthening particles. Fig. 12 provides SEM images of the fracture surface after testing at 150 and 450°C. In the non-irradiated state, see Fig. 12(a), there is excessive post-necking deformation leading to nearly neck-to-edge fracture surface. The fracture occurs by dimple rupture and shear, and nearly the

same deformation pattern is observed at 450°C. The sample irradiated at 450°C and tested at 150°C also shows quite significant post-necking deformation, see Fig. 12(b), although the reduction area is smaller. The fracture mode remains the same as before the irradiation i.e. dimple rupture. The tests performed at 450°C yielded to practically no post-necking deformation, as is shown in Fig. 12(c) and (d) for the two samples whose stress-strain responses are provided in Fig. 9(d). Very low UTS as well as negligible post necking deformation at 450°C is quite unexpected given a good ductility observed on the same set of samples at 150°C.

4. SUMMARY AND OUTLOOK

The present contribution covers two major topics: (i) embrittlement of pure W and advanced W alloys under neutron irradiation performed in wide temperature range up to 1200°C – corresponding to the surface temperature of divertor PFCs in the high flux region under steady-state operational conditions; (ii) strength and ductility of advanced Cu-alloys/composites under operational conditions in a water-cooled divertor scenario and exploring a possibility to extend the operational temperature window in the upper range from 300-350°C to 450°C, otherwise limited by irradiation softening and creep taking place in the ITER baseline CuCrZr alloy.

A major step forward has been realized in terms of the assessment of the neutron irradiation exposure on engineering-relevant mechanical properties (such as fracture toughness) at high temperature. For the commercially pure baseline W (for T-L orientation), the threshold boundary for ductile operation lies in the range between 900-1100°C, as determined on the basis of fracture toughness and bending tests. Irradiation at lower temperatures leads to operational embrittlement (i.e. fracture toughness decreases to the lower shelf value, no ductile deformation) under an applied neutron dose of ~1 dpa and a W to Re transmutation rate of 2 at%/dpa.

Screening tests applied to a set of newly developed tungsten alloys/composites have shown that some solutions (involving K-doping and rolling) truly demonstrate an enhanced tolerance to neutron irradiation exhibiting ductile behavior below 600°C even at the lowest irradiation conditions (T_{irr} = 600°C, 1 dpa). Hence, the lower bound of the operational temperature window in which ductile performance up to 1 dpa has been registered might be reduced from 900-1100°C to 600°C. It would be important to measure the fracture toughness and tensile characteristics of the above discussed prospective materials under the same irradiation conditions as presented here.

The assessment of the tensile properties of several advanced Cu-based alloys have also revealed some prospective solutions as well as brought unexpected outcomes. W_f- and W particle-reinforced materials sustained high tensile strength after the irradiation at 450°C showing resistance against irradiation softening. CuCrZr-W_f composites have shown the irradiation hardening, however, W fibers sustain ductile deformation ability even at the lower limit test temperature conditions. Cu-ODS material has shown moderate irradiation hardening accompanied with the reduction of the total elongation. In the case of W-particle materials, the reduction of the uniform and even total elongation was considerable at each studied temperature. The originally promising CuCrZr-W laminates were found to exhibit brittle deformation at every combination of the irradiation/test condition studied. The irradiation softening and strong reduction of the reduction area has been revealed in the V-alloyed CuCrZr after irradiation at 450°C, which has not been expected either.

To finalize, we bring an outlook for future studies which will require both fundamental understanding of irradiation damage as well as seeking for new technological solutions. An unexpected irradiation embrittlement of W-Cu laminates requires detailed microstructural investigation of the W-Cu interfaces as cracks were seen to initiate from those regions. Understanding the irradiation effect on the W-Cu interface is of general interest for the ITER PFCs. Currently, it is unclear whether the same severe damage would occur on the macroscopic W-Cu-CuCrZr joint. High resolution TEM and atom probe investigations are of high relevance for the V-alloyed CuCrZr, which revealed pronounced strength loss and decrease of the reduction area after the irradiation and testing at 450 °C. Surprisingly, the elongation at 150°C is much higher than at 450°C, pointing at some interplay between the irradiation microstructure and plastic deformation mechanisms (e.g. thermally activated plastic deformation removes the irradiation defects causing the observed softening, possibly coupled with dislocation channelling).

Further optimization of the PIM fine-grain structured tungsten is needed to reduce the DBTT in the non-irradiated state. The performance of the Cu-W_f composites is found promising, yet the endurance of the W fibers under neutron exposure in terms of ductility exhaustion is a very important question to be answered for both W- and Cu-based composites.

Depending on the specific location of tungsten, the transmutation rate and accumulation of Re and Os will differ. Alloying of W by Re (without applying neutron irradiation) demonstrates an improvement in terms of DBTT reduction without compromising high temperature performance [20]. However, the interplay of transmutation and irradiation damage accumulation as well as irradiation-induced secondary phase formation [35, 39] in the Re-added alloys needs to be investigated further. The two effects may counter-act each other depending on the irradiation temperature, fluence and spectrum, which would differ for the plasma-facing side of W block and the one behind the cooling pipe.

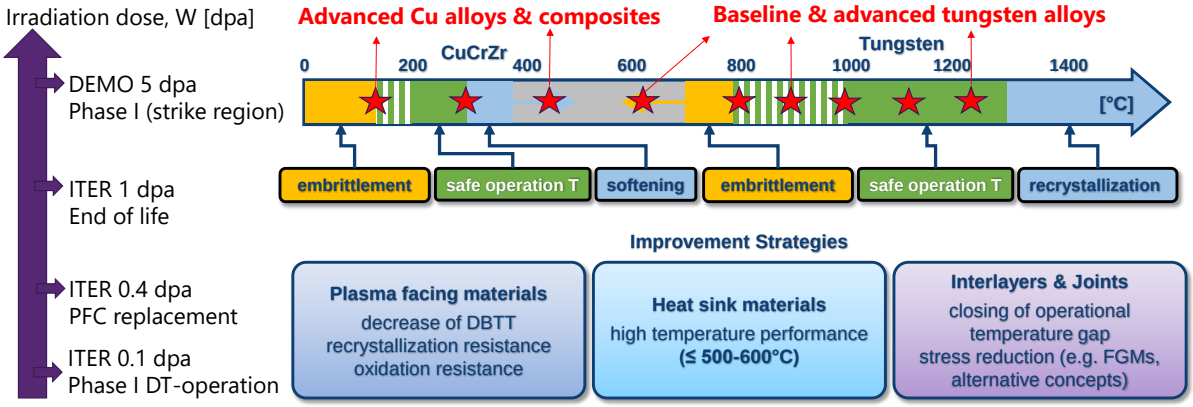

FIG.1. EU programme on irradiation testing of high heat flux materials.

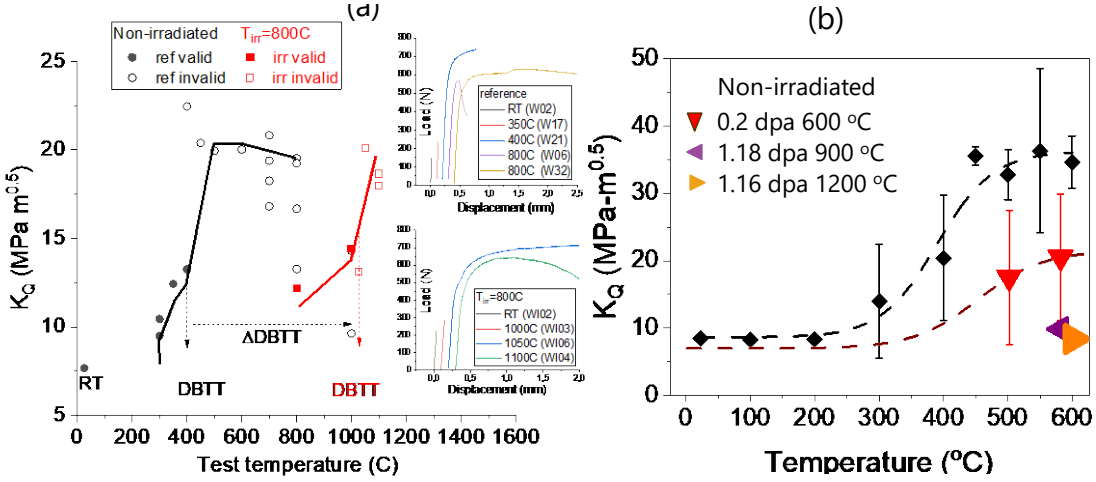

FIG.2. Assessment of irradiation embrittlement in pure tungsten (baseline material).(a) fracture toughness after irradiation at 800°C 1dpa, in-depth study is presented in [13]; (b) fracture toughness after irradiation at 600, 900 and 1200°C.

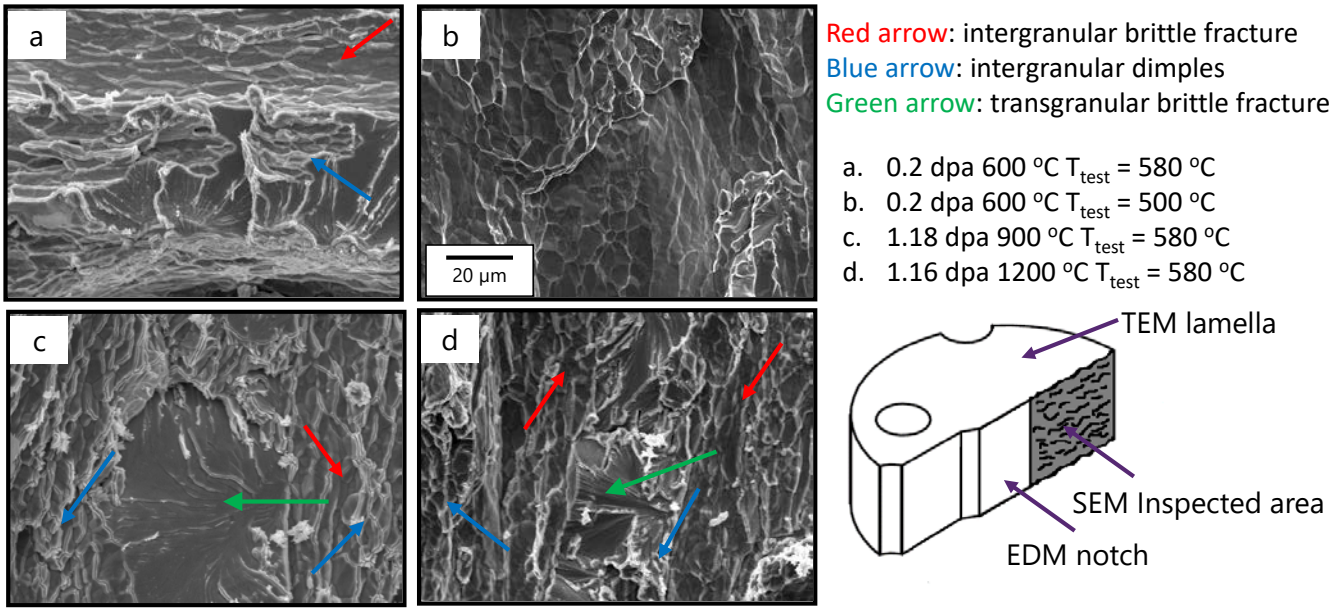

FIG.3. Examples of SEM images of the fracture surface taken from the fracture toughness samples. The irradiation conditions are shown on the legend. The inspected area and region for the extraction of TEM sample are shown schematically in the lower right corner.

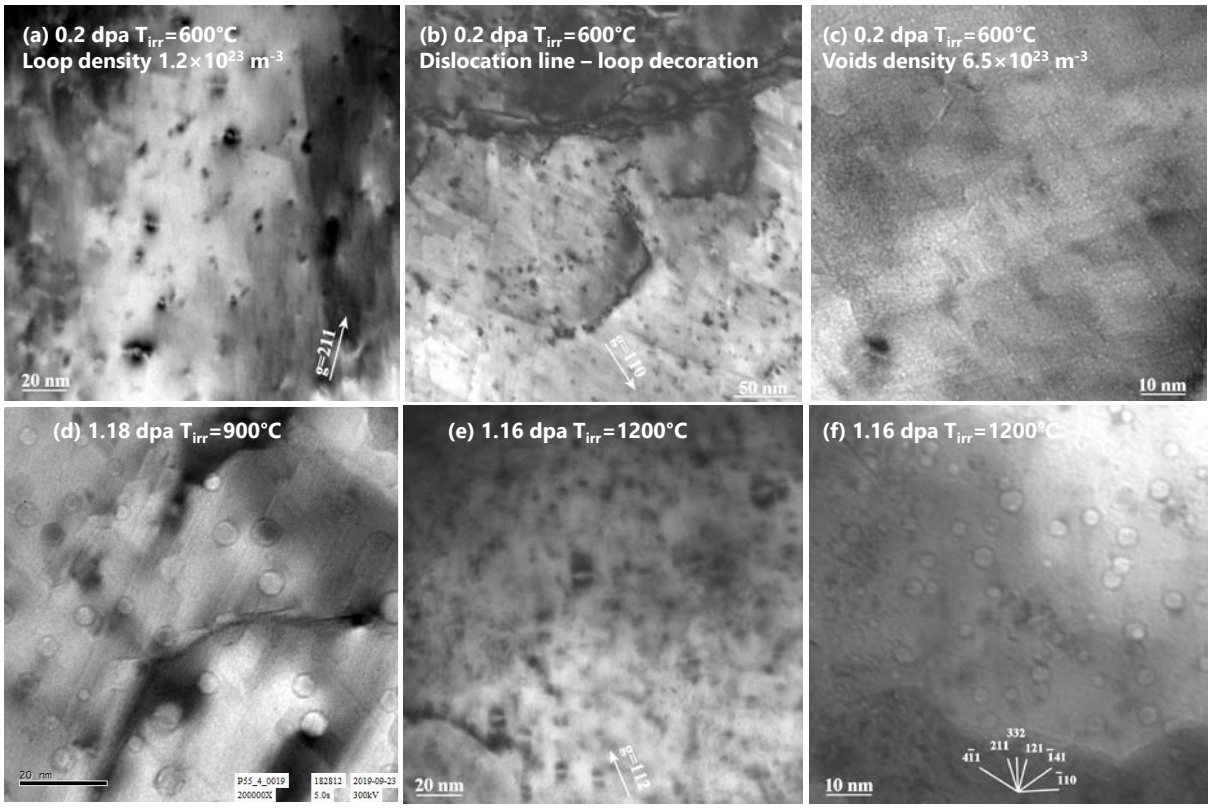

Fig.4. Examples of TEM images of the irradiation defects on the TEM lamellas extracted from the fracture toughness samples tested at 580°C after 600°C, 900°C and 1200°C irradiation.

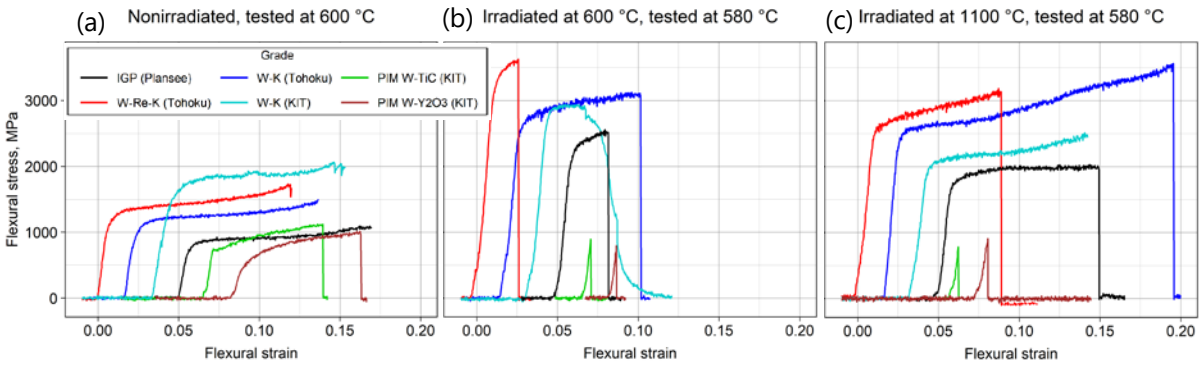

Fig.5. Comparison of 3PB load-displacement curves obtained for the advanced W materials in (a) non-irradiated state; (b) irradiated at 600°C at 1 dpa; (d) irradiated at 1100°C at 1 dpa.

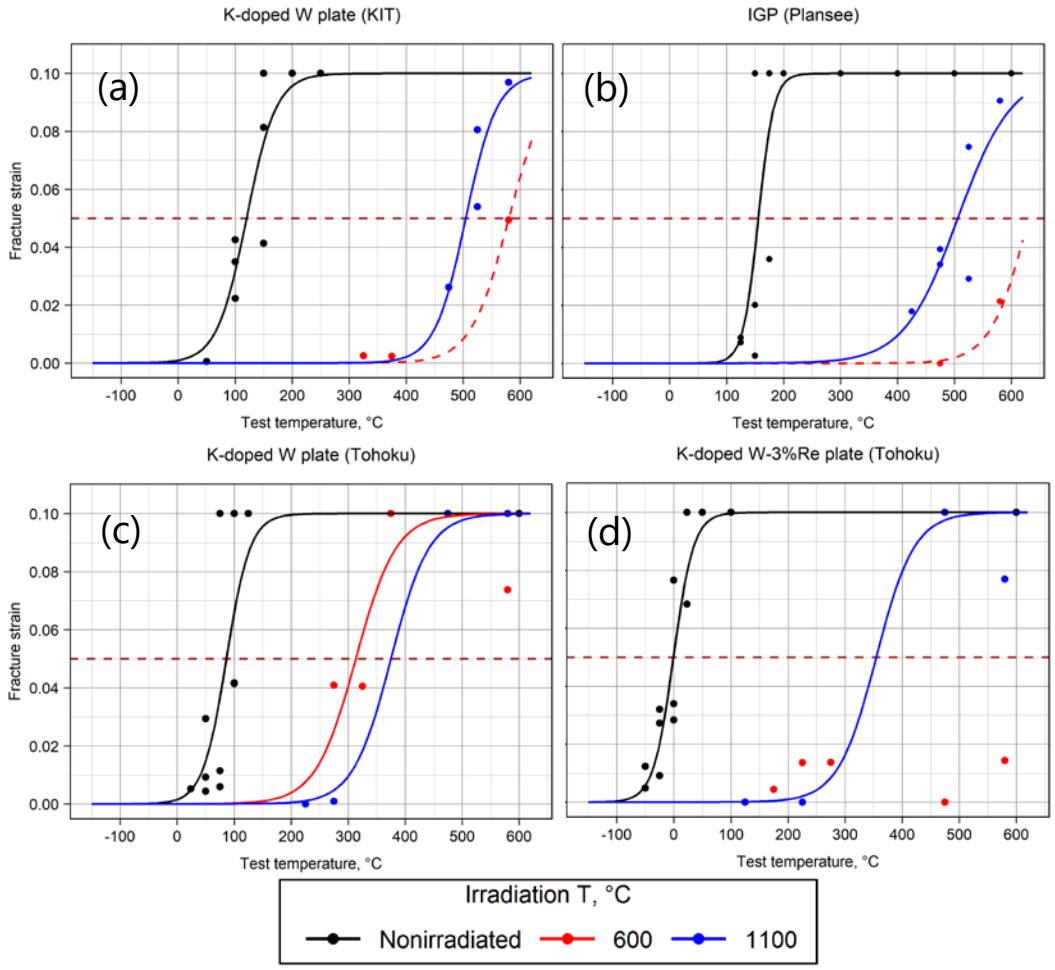

Fig.6. Derivation of DBTT for the advanced W materials using flexural strain at fracture values.

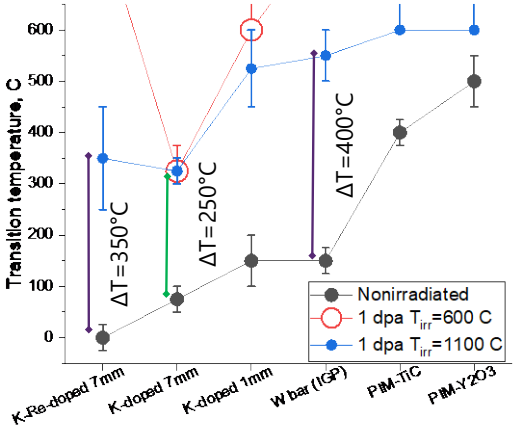

Fig.7. DBTT for the advanced and baseline W materials after irradiation at 600 and 1100°C at 1 dpa.

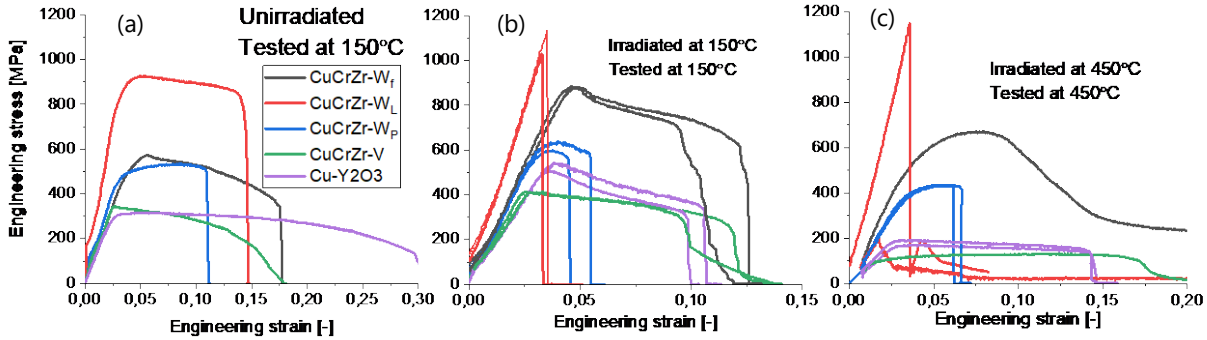

Fig.8. Engineering stress-strain curves for the advanced Cu alloys in (a) non-irradiated state tested at 150°C; (b) irradiated and tested at 150°C; (c) irradiated and tested at 450°C.

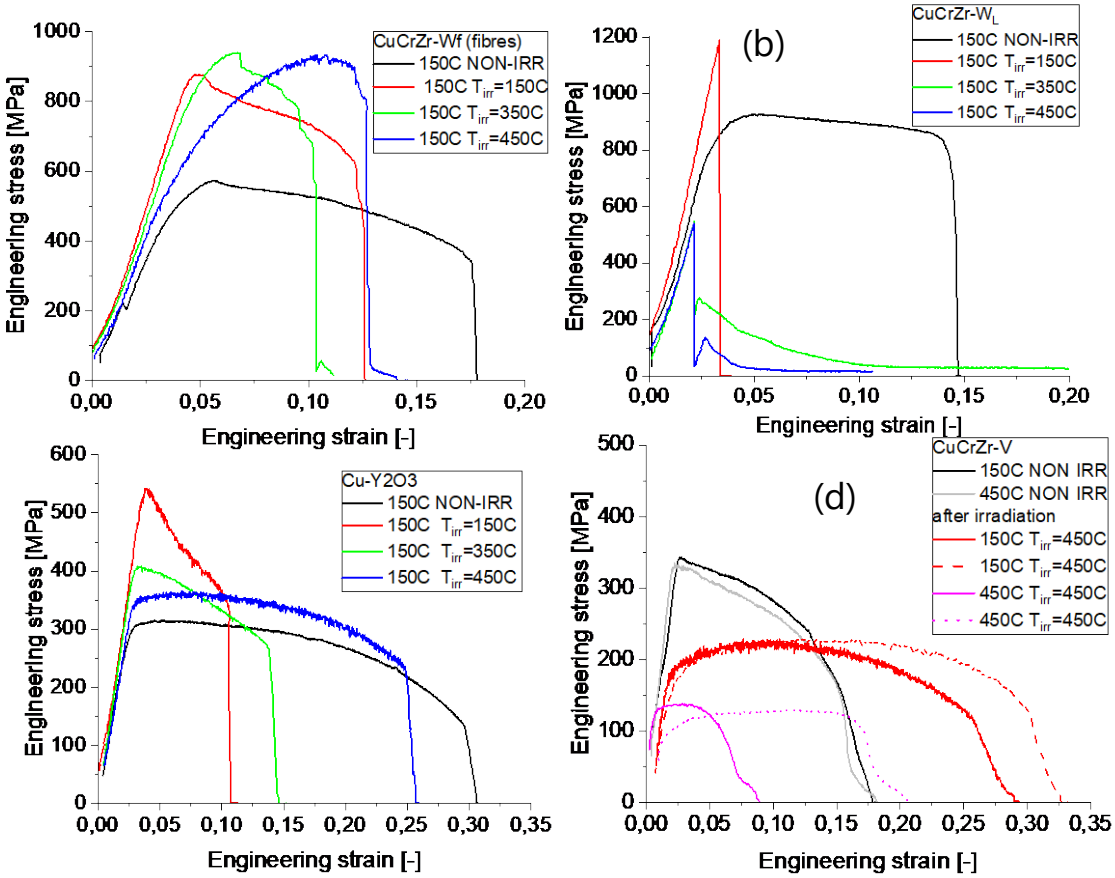

Fig.9. Engineering stress-strain curves for the advanced Cu alloys. The type of material, irradiation and test temperatures are provided on the corresponding legends.

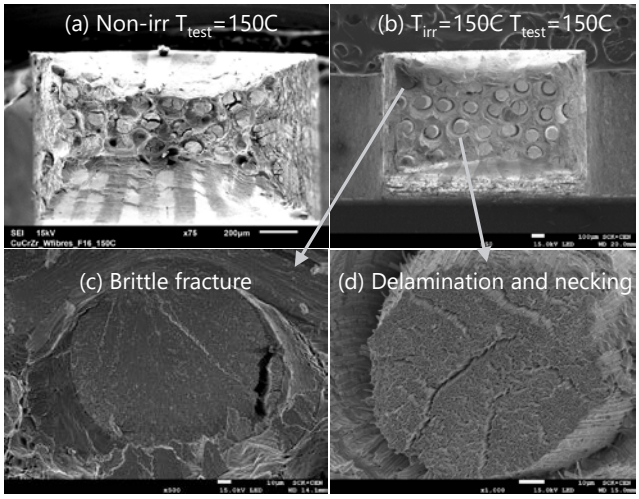

Fig.10. Fracture surface of the CuCrZr-Wf composites T_{irr}=T_{test}=150°C.

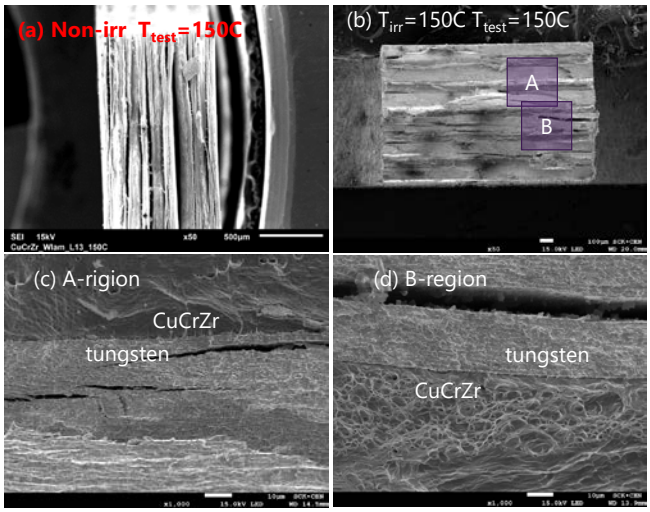

Fig.11. Fracture surface of the CuCrZr-W laminate composites T_{irr}=T_{test}=150°C.

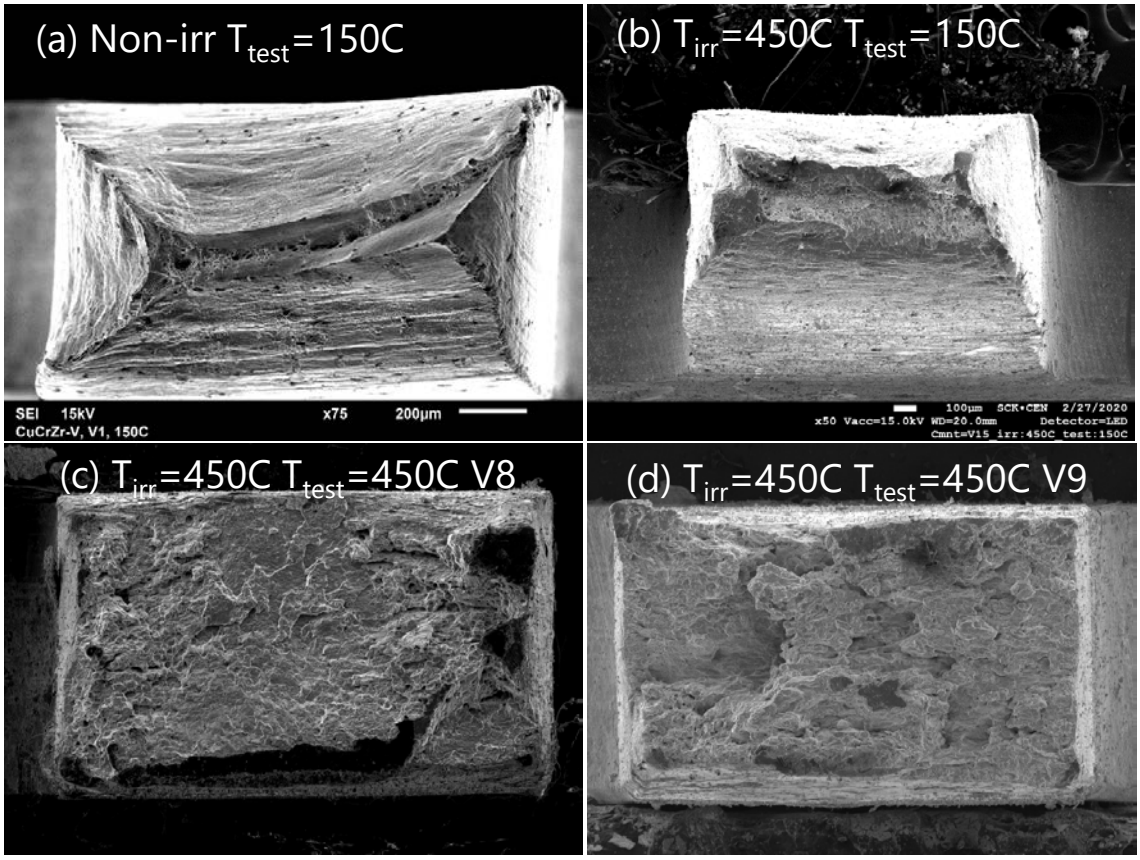

Fig.12. Fracture surface of the CuCrZr-V T_{irr}=450°C tested at 150 and 450°C.

ACKNOWLEDGEMENTS

This work has been carried out within the framework of the EUROfusion Consortium and has received funding from the Euratom research and training programme 2014-2018 and 2019-2020 under grant agreement No 633053. The views and opinions expressed herein do not necessarily reflect those of the ITER Organization or of the European Commission.

REFERENCES

[1] G. Pintsuk, E. Diegele, S.L. Dudarev, M. Gorley, J. Henry, J. Reiser, M. Rieth, European materials development: Results and perspective, Fusion Engineering and Design 146 (2019) 1300-1307.
[2] M. Rieth, R. Doerner, A. Hasegawa, Y. Ueda, M. Wirtz, Behavior of tungsten under irradiation and plasma interaction, Journal of Nuclear Materials 519 (2019) 334-368.
[3] V. Barabash, G. Federici, M. Rodig, L.L. Snead, C.H. Wu, Neutron irradiation effects on plasma facing materials, Journal of Nuclear Materials 283 (2000) 138-146.
[4] V.R. Barabash, G.M. Kalinin, S.A. Fabritsiev, S.J. Zinkle, Specification of CuCrZr alloy properties after various thermo-mechanical treatments and design allowables including neutron irradiation effects, Journal of Nuclear Materials 417(1-3) (2011) 904-907.
[5] J.H. You, E. Visca, C. Bachmann, T. Barrett, F. Crescenzi, M. Fursdon, H. Greuner, D. Guilhem, P. Languille, M. Li, S. McIntosh, A.V. Muller, J. Reiser, M. Richou, M. Rieth, European DEMO divertor target: Operational requirements and material-design interface, Nuclear Materials and Energy 9 (2016) 171-176.
[6] D. Pelowitz, J. Durkee, J. Elson, M. Fensin, M. James, R. Johns, G. McKinney, S. Mashnik, L. Waters, T. Wilcox, MCNPX 2.7. 0 Extensions, Los Alamos National Laboratory, 2011.
[7] S.L. Dudarev, DPA definition and estimates, 2015. https://www-amdis.iaea.org/CRP/IrradiatedTungsten/RCM2/RCM2Presentation-DudarevDPA-2015-09-10.pdf.
[8] A. Stankovskiy, G. Van den Eynde, L. Fiorito, ALEPH V.2.7, A Monte Carlo Burn-Up Code, SCK•CEN, 2018.
[9] A. Plompen, et al., JEFF-3.3, Nuclear Energry Agency, 2017.
[10] D.A. Brown, M. Chadwick, R. Capote, A. Kahler, A. Trkov, M. Herman, A. Sonzogni, Y. Danon, A. Carlson, M. Dunn, ENDF/B-VIII. 0: the 8th major release of the nuclear reaction data library with CIELO-project cross sections, new standards and thermal scattering data, Nuclear Data Sheets 148 (2018) 1-142.
[11] A.Y. Konobeyev, U. Fischer, Y.A. Korovin, S. Simakov, Evaluation of effective threshold displacement energies and other data required for the calculation of advanced atomic displacement cross-sections, Nuclear Energy and Technology 3(3) (2017) 169-175.
[12] M. Norgett, M. Robinson, I. Torrens, A proposed method of calculating displacement dose rates, Nuclear engineering and design 33(1) (1975) 50-54.
[13] E. Gaganidze, A. Chauhan, H.-C. Schneider, D. Terentyev, G. Borghmans, J. Aktaa, Fracture-mechanical properties of neutron irradiated ITER specification tungsten, Journal of Nuclear Materials 547 (2021) 152761.
[14] C. Yin, D. Terentyev, T. Pardoen, R. Petrov, Z.F. Tong, Ductile to brittle transition in ITER specification tungsten assessed by combined fracture toughness and bending tests analysis, Mat Sci Eng a-Struct 750 (2019) 20-30.
[15] C. Yin, D. Terentyev, T. Pardoen, A. Bakaeva, R. Petrov, S. Antusch, M. Rieth, M. Vilemova, J. Matejicek, T. Zhang, Tensile properties of baseline and advanced tungsten grades for fusion applications, Int J Refract Met H 75 (2018) 153-162.
[16] ASTM, E290 -14, Standard Test Methods for Bend Testing of Material for Ductility, E290 -14, ASTM international (2014).
[17] ASTM, Standard test method for linear-elastic plane strain fracture toughness KIC of metallic materials, E 399-12, ASTM international, 2012.
[18] M. Wirtz, J. Linke, T. Loewenhoff, G. Pintsuk, I. Uytdenhouwen, Thermal shock tests to qualify different tungsten grades as plasma facing material, Physica Scripta T167 (2016) 014015.
[19] S. Nogami, A. Hasegawa, M. Fukuda, M. Rieth, J. Reiser, G. Pintsuk, Mechanical properties of tungsten: Recent research on modified tungsten materials in Japan, Journal of Nuclear Materials 543 (2021).
[20] S. Nogami, A. Hasegawa, M. Fukuda, S. Watanabe, J. Reiser, M. Rieth, Tungsten modified by potassium doping and rhenium addition for fusion reactor applications, Fusion Engineering and Design 152 (2020).
[21] S. Antusch, D. Armstrong, B. Britton, L. Commin, J. Gibson, H. Greuner, J. Hoffmann, W. Knabl, G. Pintsuk, M. Rieth, S. Robert, T. Weingaertner, Mechanical and microstructural investigations of tungsten and doped tungsten materials produced via powder injection molding, Nuclear Materials and Energy 3-4 (2015) 22-31.
[22] J. Reiser, S. Wurster, J. Hoffmann, S. Bonk, C. Bonnekoh, D. Kiener, R. Pippan, A. Hoffmann, M. Rieth, Ductilisation of tungsten (W) through cold-rolling: R-curve behaviour, Int J Refract Met H 58 (2016) 22-33.
[23] J. Reiser, L. Garrison, H. Greuner, J. Hoffmann, T. Weingartner, U. Jantsch, M. Klimenkov, P. Franke, S. Bonk, C. Bonnekoh, S. Sickinger, S. Baumgartner, D. Bolich, M. Hoffmann, R. Ziegler, J. Konrad, J. Hohe, A. Hoffmann, T. Mrotzek, M. Seiss, M. Rieth, A. Moslang, Ductilisation of tungsten (W): Tungsten laminated composites, Int J Refract Met H 69 (2017) 66-109.
[24] J. Reiser, M. Rieth, A. Moslang, B. Dafferner, A. Hoffmann, X.O. Yi, D.E.J. Armstrong, Tungsten foil laminate for structural divertor applications - Tensile test properties of tungsten foil, Journal of Nuclear Materials 434(1-3) (2013) 357-366.

[25] A.V. Muller, B. Boswirth, V. Cerri, H. Greuner, R. Neu, U. Siefken, E. Visca, J.H. You, Application of tungsten-copper composite heat sink materials to plasma-facing component mock-ups, Physica Scripta T171(1) (2020).
[26] A. Von Muller, D. Ewert, A. Galatanu, M. Milwich, R. Neu, J.Y. Pastor, U. Siefken, E. Tejado, J.H. You, Melt infiltrated tungsten-copper composites as advanced heat sink materials for plasma facing components of future nuclear fusion devices, Fusion Engineering and Design 124 (2017) 455-459.
[27] J.W. Coenen, Y. Mao, S. Sistla, A.V. Muller, G. Pintsuk, M. Wirtz, J. Riesch, T. Hoeschen, A. Terra, J.H. You, H. Greuner, A. Kreter, C. Broeckmann, R. Neu, C. Linsmeier, Materials development for new high heat-flux component mock-ups for DEMO, Fusion Engineering and Design 146 (2019) 1431-1436.
[28] J.H. You, A. Brendel, S. Nawka, T. Schubert, B. Kieback, Thermal and mechanical properties of infiltrated W/CuCrZr composite materials for functionally graded heat sink application, Journal of Nuclear Materials 438(1-3) (2013) 1-6.
[29] B. Gludovatz, S. Wurster, A. Hoffmann, R. Pippan, Fracture toughness of polycrystalline tungsten alloys, Int J Refract Met H 28(6) (2010) 674-678.
[30] M. Faleschini, H. Kreuzer, D. Kiener, R. Pippan, Fracture toughness investigations of tungsten alloys and SPD tungsten alloys, Journal of Nuclear Materials 367 (2007) 800-805.
[31] E. Gaganidze, D. Rupp, J. Aktaa, Fracture behaviour of polycrystalline tungsten, Journal of Nuclear Materials 446(1-3) (2014) 240-245.
[32] A. Hasegawa, M. Fukuda, K. Yabuuchi, S. Nogami, Neutron irradiation effects on the microstructural development of tungsten and tungsten alloys, Journal of Nuclear Materials 471 (2016) 175-183.
[33] A. Hasegawa, M. Fukuda, T. Tanno, S. Nogami, Neutron Irradiation Behavior of Tungsten, Materials Transactions 54(4) (2013) 466-471.
[34] D. Terentyev, C. Yin, A. Dubinko, C.C. Chang, J.H. You, Neutron irradiation hardening across ITER diverter tungsten armor, Int J Refract Met H 95 (2021).
[35] M. Klimenkov, U. Jantsch, M. Rieth, H.C. Schneider, D.E.J. Armstrong, J. Gibson, S.G. Roberts, Effect of neutron irradiation on the microstructure of tungsten, Nuclear Materials and Energy 9 (2016) 480-483.
[36] D.H. Lassila, F. Magness, D. Freeman, Ductile-Brittle Transition Temperature Testing of Tungsten Using the Three-Point Bend Test, Report Lawrence Livermore National Laboratory UCRL-ID-108258 (1991).
[37] D. Terentyev, W. Van Renterghem, L. Tanure, A. Dubinko, J. Riesch, S. Lebediev, T. Khvan, K. Verbeken, J.W. Coenen, E.E. Zhurkin, Correlation of microstructural and mechanical properties of K-doped tungsten fibers used as reinforcement of tungsten matrix for high temperature applications, Int J Refract Met H 79 (2019) 204-216.
[38] L.M. Garrison, Y. Katoh, L.L. Snead, T.S. Byun, J. Reiser, M. Rieth, Irradiation effects in tungsten-copper laminate composite, Journal of Nuclear Materials 481 (2016) 134-146.
[39] X.X. Hu, C.M. Parish, K. Wang, T. Koyanagi, B.P. Eftink, Y. Katoh, Transmutation-induced precipitation in tungsten irradiated with a mixed energy neutron spectrum, Acta Materialia 165 (2019) 51-61.